Article

Not peer-reviewed version

Bicarbazole-benzophenone based twisted donor-acceptor derivatives as potential blue emitters for OLEDs

Iram Siddiqui , Prakalp Gautam , Dovydas Blazevicius , Jayakumar Jayakumar , Sushanta Lenka ,
Daiva Tavgeniene , Ernestas Zaleckas , Jwo-Huei Jou , Saulius Grigalevicius *

Posted Date: 7 March 2024

doi: 10.20944/preprints202403.0382.v1

Keywords: donor-acceptor derivatives; blue organic light emitting diode; high efficiency; blue emission; thermal analysis

Article

Bicarbazole-Benzophenone Based Twisted Donor-Acceptor Derivatives as Potential Blue Emitters for OLEDs

Iram Siddiqui [1,†], Prakalp Gautam [1], Dovydas Blazevicius [2,†], Jayakumar Jayachandran [1], Sushanta Lenka [1], Daiva Tavgeniene [2], Ernestas Zaleckas [3], Saulius Grigalevicius [2,*] and Jwo-Huei Jou [1,*]

[1] Department of Materials Science and Engineering, National Tsing Hua University, Hsinchu 30044, Taiwan; iramsidd29@gmail.com (I.S.); prakalpgautam@gmail.com (P.G.); jayakumar@mx.nthu.edu.tw (J.J.); sushantalenka1@gmail.com (S.L.)

[2] Department of Polymer Chemistry and Technology, Kaunas University of Technology, Radvilenu plentas 19, Kaunas, LT50254, Lithuania; dovydas.blazevicius@ktu.lt (D.B.); daiva.tavgeniene@ktu.lt (D.T.)

[3] Vytautas Magnus University, Agriculture Academy, Department of Agricultural Engineering and Safety, Studentu str. 11, LT-53361, Akademija, Kaunas distr., Lithuania; ernestas.zaleckas@vdu.lt (E.Z.).

* Correspondence: Correspondence: saulius.grigalevicius@ktu.lt (S.G.); jjou@mx.nthu.edu.tw (J.-H.J.)

† These authors contributed equally to this work.

Abstract: We designed twisted donor-acceptor type electroactive bipolar derivatives that used benzophenone and bicarbazole as building blocks. Derivatives were synthesized through the reaction of 4-fluorobenzophenone with various partially alkylated 3,3′-bicarbazoles. The comprehensive structural characterization of these compounds is provided. These amorphous materials exhibit suitable glass transition temperatures ranging from 57 to 102 °C and demonstrate high thermal stability, with decomposition temperatures reaching 400 °C. Moreover, the developed materials exhibit elevated photoluminescence quantum yields (PLQY) of up to 75.5% and favorable HOMO-LUMO levels, along with suitable triplet-singlet state energy values. Due to their good solubility and suitable film-forming properties, all the compounds were evaluated as blue emitters in tandem with commercial 4,4′-bis(N-carbazolyl)-1,10-biphenyl (CBP) host material in emissive layer of organic light-emitting diodes (OLEDs) in concentration dependent experiments. Out of these experiments, the OLED with 15 wt% of the emitting derivative 4-(9′-{2-ethylhexyl}-[3,3′]-bicarbazol-9-yl)benzophenone exhibited superior performance. It attained a maximum brightness of 3581 cd/m^2, current efficacy of 5.7 cd/A, power efficacy of 4.1 lm/W, and an external quantum efficacy of 2.7%.

Keywords: donor-acceptor derivatives; blue organic light emitting diode; high efficiency; blue emission; thermal analysis

1. Introduction

In recent decades, there has been significant and swift advancement in organic light-emitting diode (OLED) technology, transforming it into a multi-billion-dollar market [1]. Its applications have expanded across various domains, encompassing high-contrast flat-panel displays, smartwatches, smartphones, and big-screen television sets. Also, solid-state lighting is attracting growing interest in both industrial and scientific domains [2–7]. OLED devices present superior features such as colour purity, reduced weight, lower power consumption, faster response and flexibility, surpassing capabilities offered by existing technologies [8–11].

Until now, the prevailing commercial OLED devices have primarily relied on phosphorescent materials containing noble metals like platinum and iridium [12]. Yet, incorporating atoms of noble metals into structures of phosphorescent materials presents a notable obstacle not only to the future manufacturing expenses of devices, but also prompts environmental concerns [13,14]. Moreover, there is a tendency for the nonradiative transition rate of phosphorescent metal complexes d-orbitals to increase when the emission peaks are shifting to the blue region of emission, posing challenges in achieving both high efficiency and stability in blue phosphorescent OLEDs [15–20]. In an effort to address these challenges, there is a renewed focus on the development of small-molecule fluorescent materials, primarily due to their high colour purity and cost-effectiveness [21]. In recent years, there has been considerable attention focused on thermally activated delayed fluorescence (TADF) materials. This is due to absence of metal atoms in their structures and their capability to employ reverse intersystem crossing (RISC), resulting in the upconversion of triplet excitons to emissive singlet excitons, leading to significantly enhanced external quantum efficiencies (EQEs) [22–28]. However, numerous TADF OLEDs face challenges including triplet-triplet and singlet-triplet annihilation, as well as concentration quenching. These issues can be attributed to prolonged exciton lifetimes, leading to a notable decrease in efficiency as luminance increases [29–31].

A crucial requirement for TADF OLED emitters to function efficiently is achieving the smallest possible singlet-triplet energy differential (ΔE_{ST}). This can be accomplished through molecular design strategies aimed at maximizing the separation between the highest occupied molecular orbital (HOMO) and the lowest unoccupied molecular orbital (LUMO). One effective approach is the incorporation of highly twisted donor and acceptor structured frameworks [30,32,33]. The distinct attributes of benzophenone and its derivatives, such as potent electron-withdrawing capabilities, effective intersystem crossing due to robust spin-orbit coupling, and a twisted configuration, hold promise for advancing the creation of efficient TADF emitters with shortened exciton lifetimes via a smart molecular design approach [34–42]. Carbazole, widely recognized for its electron-rich nature, has been extensively employed as an electron donor in a wide range of optoelectronic devices, serving for both host materials and emitters in various configurations. This is due to its capacity for facile functionalization across multiple sites, adjustable electronic and optical properties, robust electrochemical and thermal stability, and a high photoluminescence quantum yield [43–49]. Materials exhibiting both favourable film-forming properties and solubility in common organic solvents are extensively explored in scientific research and technological development. This interest stems from the fact that low molar mass organic derivatives, also called molecular glasses, demonstrate capability to form transparent, stable, and homogenous amorphous layers in devices [50,51]. Solubility in common organic solvents of new materials enables solution-based manufacturing processes, such as blade or spin coating, and inkjet printing, which are simpler, cost-effective and more scalable than usual vacuum evaporation method [52–55].

In this study, we present the synthesis, investigation and application of new electroactive compounds that feature benzophenone and 3,3′-bicarbazole fragments acting as electron acceptor and as an electron donor, respectively, within donor-acceptor type twisted molecules and explore their utility as blue emitters in organic LEDs. The selection of alkyl sidechains, including ethyl, butyl, pentyl, hexyl, 2-ethylhexyl, and octyl was aimed to optimizing their film-forming properties, solubility, and, consequently, solution process-ability [56].

2. Experimental Part

2.1. Instrumentation

The recording of ^{1}H and ^{13}C nuclear magnetic resonance (NMR) spectra was conducted with the Bruker Avance III (400 MHz) instrument. Chemical shifts (δ, ppm) are presented relative to trimethylsilane standard. Acquisition of mass spectra were achieved using the Waters ZQ 2000 mass spectrometer. Thermogravimetric analysis (TGA) was carried out utilizing the TGAQ50 analyser, while thermograms of differential scanning calorimetry (DSC) were recorded using the Bruker Reflex II DSC apparatus. For both types of thermal analysis, a heating rate of 10 ^{o}C/min in a nitrogen atmosphere was selected. Ultraviolet–visible (UV-vis) spectroscopy involved an HP-8453 diode array spectrometer to measure compound absorption spectra, and the resultant absorbance wavelengths were used to generate Tauc plot. Aminco-Bowman Series 2 spectrofluorometer was used to record photoluminescence (PL) spectra. Low-temperature PL (LTPL) spectra at 77K to determine triplet energy was recorded with a Hitachi F-7000 fluorescence spectrophotometer. The CH instrument CH1604A potentiostat was used to perform cyclic voltammetry (CV), and based on these results, HOMO levels were calculated. Time-resolved photoluminescence (TRPL) experiments, aiming to determine compound decay time, were conducted with an Edinburgh instrument FLS980 spectrometer.

2.2. Synthesis and Structural Analysis

Carbazole (1), 1-bromooctane, 2-ethylhexylbromide, 1-bromohexane, 1-bromopentane, 1-bromobutane, bromoethane, FeCl$_3$, KOH, K$_2$CO$_3$, Na$_2$SO$_4$, 4-fluorobenzophenone, chloroform, dimethyl sulfoxide (DMSO) and tetrahydrofuran (THF) were bought from Aldrich and used without further purification.

9H,9‘H-3,3’-Bicarbazole (2) was synthesized using 9H-carbazole as a starting material and FeCl$_3$ as an oxidising agent, as it was described earlier [57].

9-Ethyl-9‘H-3,3’-bicarbazole (3) was synthesized by partially alkylating 9H,9‘H-3,3’-bicarbazole (2) as it was described previously [58].

9-Butyl-9‘H-3,3’-bicarbazole (4) was also synthesized by partially alkylating 9H,9‘H-3,3’-bicarbazole (2) as it was described previously [58].

9-Pentyl-9‘H-3,3’-bicarbazole (5). 9H,9‘H-3,3’-bicarbazole (2) (2.00 g, 6.02 mmol) was dissolved in 50 ml of tetrahydrofuran, and 1-bromopentane (0.91 g, 6.02 mmol) was subsequently added. Potassium carbonate (1.66 g, 12.04 mmol) and powdered potassium hydroxide (2.02 g, 36.12 mmol) were gradually introduced while the solution was stirred continuously and heated to boiling temperature. After 4 hours, TLC analysis was conducted, and the solution was filtered using a paper filter. The pure product was then isolated through column chromatography using tetrahydrofuran/hexane (volume ratio 1:5) as the mobile phase and silica gel as the stationary phase. The yield obtained was 1.06 g (44%) of pale-yellow material. ^{1}H NMR (400 MHz, CDCl$_3$, δ, m.d.): 8.47 (d, 2H, J = 10 Hz), 8.26 (d, 1H, 7.6 Hz), 8.23 (d, 1H, 8.0 Hz), 7.96 (s, 1H), 7.88 (d, 1H, J = 8.4 Hz), 7.84 (dd, 1H, J$_1$ = 8.4 Hz, J$_2$ = 1.6 Hz), 7.58-7.53 (m, 2H), 7.50-7.47 (m, 3H), 7.43 (d, 1H, J = 8 Hz), 7.33 (t, 2H, J = 7.2 Hz), 4.37 (t, 2H, J = 7,0 Hz), 1.96 (qu, 2H, J = 7.2 Hz), 1.49-1.41 (m, 4H), 0.96 (t, 3H, J = 7.2 Hz). ^{13}C NMR (101 MHz, CDCl$_3$, δ, m.d.): 140.98, 140.04, 139.65, 138.56, 133.33, 125.95, 125.87, 125.75, 125.60, 124.00, 123.61, 123.44, 123.10, 120.53, 120.47, 119.52, 119.02, 118.91, 118.83, 110.86, 110.79, 108.97, 108.87, 43.23, 29.50, 28.81, 22.58, 14.05.

9-Hexyl-9‘H-3,3’-bicarbazole (6). 9H,9‘H-3,3’-bicarbazole (2) (2.00 g, 6.02 mmol) was dissolved in 50 ml of tetrahydrofuran, and 1-bromohexane (0.99 g, 6.02 mmol) was subsequently added. Potassium carbonate (1.66 g, 12.04 mmol) and powdered potassium hydroxide (2.02 g, 36.12 mmol) were gradually introduced while the solution was stirred continuously and heated to boiling temperature. After 4 hours, TLC analysis was conducted, and the solution was filtered using a paper filter. The pure product was then isolated through column chromatography using tetrahydrofuran/hexane (volume ratio 1:7) as the mobile phase and silica gel as the stationary phase. The yield obtained was 1.00 g (40%) of pale-yellow material. ^{1}H NMR (400 MHz, CDCl$_3$, δ, m.d.): 8.46 (d, 2H, J = 9.8 Hz), 8.25 (d, 1H, J = 8.0 Hz), 8.22 (d, 1H, J = 7.6 Hz), 7.99 (s, 1H), 7.88 (dd, 1H, J$_1$ = 8.4 Hz, J$_2$ = 1.6 Hz), 7.83 (dd, 1H, J$_1$ = 8.4 Hz, J$_2$ = 2.0 Hz), 7.57-7.43 (m, 6H), 7.32 (t, 2H, J = 7.4 Hz), 4.37 (t, 2H, J = 7.2 Hz), 1.95 (qu, 2H, J = 7.4 Hz), 1.50-1.33 (m, 6H), 0.94 (t, 3H, J = 7.2 Hz). ^{13}C NMR (101 MHz, CDCl$_3$, δ, m.d.): 140.97, 140.03, 139.64, 138.55, 134.13, 133.32, 125.95, 125.87, 125.73, 125.58, 124.00, 123.61, 123.44, 123.10, 120.51, 120.46, 119.51, 119.01, 118.91, 118.81, 110.83, 110.76, 108.95, 108.85, 43.26, 31.67, 29.05, 27.06, 22.62, 14.10.

9-(2-Ethylhexyl)-9‘H-3,3’-bicarbazole (7) was synthesized by partially alkylating 9H,9‘H-3,3’-bicarbazole (2) as it was described previously [58].

9-Octyl-9‘H-3,3’-bicarbazole (8) was synthesized by partially alkylating 9H,9‘H-3,3’-bicarbazole (2) as it was described previously [59].

4-(9’-Ethyl-[3,3’]-bicarbazol-9-yl)benzophenone (DB41) was synthesized by stirring 9-ethyl-9‘H-3,3’-bicarbazole (3) (0.50 g, 1.39 mmol) with 4-fluorobenzophenone (0.28 g, 1.39 mmol) in 10 ml of

DMSO at 150 °C under an inert nitrogen atmosphere with potassium carbonate (1.92 g, 13.90 mmol) present. After 4 hours, TLC was used to confirm the completion of the reaction, following which the reaction mixture was slowly added to ice water. Chloroform was employed to extract the organic phase, and any remaining water traces in the organic phase were removed by adding anhydrous Na_2SO_4, which was filtered off later. The desired product was purified via column chromatography using tetrahydrofuran/hexane (volume ratio 1:3) as the mobile phase and silica gel as the stationary phase, resulting in yellow amorphous material with a yield of 0.62 g (82%). T_g = 102 °C (DSC). ^{1}H NMR (400 MHz, $CDCl_3$, δ, m.d.): 8.48 (dd, 2H, J_1 = 11.2 Hz, J_2 = 1.6 Hz), 8.28 (d, 1H, J = 7.6 Hz), 8.24 (d, 1H, J = 7.6 Hz), 8.14 (d, 2H, J = 8.4 Hz), 7.97-7.95 (m, 1H), 7.89-7.81 (m, 4H), 7.69-7.65 (m, 2H), 7.61 (dd, 2H, J_1 = 8.0 Hz, J_2 = 1.6 Hz), 7.58-7.45 (m, 6H), 7.40 (t, 1H, J = 7.4 Hz), 7.33-7.30 (m, 1H), 4.46 (q, 2H, J = 7.2 Hz), 1.52 (t, 3H, J = 7.2 Hz). ^{13}C NMR (101 MHz, $CDCl_3$, δ, m.d.): 195.66, 141.81, 140.73, 140.46, 139.31, 139.21, 137.51, 135.97, 135.32, 132.95, 132.65, 131.95, 130.07, 128.49, 126.33, 126.21, 126.11, 125.81, 125.52, 124.51, 124.13, 123.59, 123.15, 120.69, 120.61, 120.56, 119.09, 119.00, 118.89, 110.07, 109.94, 108.73, 108.62, 37.69, 13.89. MS ($APCI^+$, 20 V): 540.26 ([M+H], 100%).

4-(9′-Butyl-[3,3′]-bicarbazol-9-yl)benzophenone (DB44) was synthesized by stirring 9-butyl-9′H-3,3′-bicarbazole (3) (0.50 g, 1.29 mmol) with 4-fluorobenzophenone (0.26 g, 1.29 mmol) in 10 ml of DMSO at 150 °C under an inert nitrogen atmosphere with potassium carbonate (1.78 g, 12.90 mmol) present. After 4 hours, TLC was used to confirm the completion of the reaction, following which the reaction mixture was slowly added to ice water. Chloroform was employed to extract the organic phase, and any remaining water traces in the organic phase were removed by adding anhydrous Na_2SO_4, which was filtered off later. The desired product was purified via column chromatography using tetrahydrofuran/hexane (volume ratio 1:5) as the mobile phase and silica gel as the stationary phase, resulting in yellow amorphous material with a yield of 0.66 g (90%). T_g = 82 °C (DSC). ^{1}H NMR (400 MHz, $CDCl_3$, δ, m.d.): 8.49 (dd, 2H, J_1 = 8.4 Hz, J_2 = 1.6 Hz), 8.29 (d, 1H, J = 7.6 Hz), 8.25 (d, 1H, J = 7.6 Hz), 8.14 (d, 2H, J = 7.2 Hz), 7.97 (d, 2H, J = 7.2 Hz), 7.89-7.84 (m, 2H), 7.82 (d, 2H, 8.4 Hz), 7.69-7.65 (m, 2H), 7.63-7.58 (m, 3H), 7.56-7.47 (m, 4H), 7.40 (t, 1H, J = 7.4 Hz), 7.31 (t, 1H, J = 7.6 Hz), 4.39 (t, 2H, J = 7.2 Hz), 1.95 (qu, 2H, J = 7.4 Hz), 1.48 (sext, 2H, J = 7.6 Hz), 1.02 (t, 3H, J = 7.4 Hz). ^{13}C NMR (101 MHz, $CDCl_3$, δ, m.d.): 196.66, 141.81, 140.98, 140.73, 139.74, 139.31, 137.53, 135.96, 135.33, 132.89, 132.66, 131.96, 130.08, 128.50, 126.34, 126.21, 126.11, 125.78, 125.49, 124.52, 124.15, 123.48, 123.04, 120.71, 120.62, 120.50, 119.01, 118.86, 110.08, 109.96, 108.99, 108.87, 43.00, 31.23, 20.64, 13.96. MS ($APCI^+$, 20 V): 568.39 ([M+H], 100%).

4-(9′-Pentyl-[3,3′]-bicarbazol-9-yl)benzophenone (DB37) was synthesized by stirring 9-pentyl-9′H-3,3′-bicarbazole (3) (0.50 g, 1.24 mmol) with 4-fluorobenzophenone (0.25 g, 1.24 mmol) in 10 ml of DMSO at 150 °C under an inert nitrogen atmosphere with potassium carbonate (1.72 g, 12.40 mmol) present. After 4 hours, TLC was used to confirm the completion of the reaction, following which the reaction mixture was slowly added to ice water. Chloroform was employed to extract the organic phase, and any remaining water traces in the organic phase were removed by adding anhydrous Na_2SO_4, which was filtered off later. The desired product was purified via column chromatography using tetrahydrofuran/hexane (volume ratio 1:5) as the mobile phase and silica gel as the stationary phase, resulting in yellow amorphous material with a yield of 0.66 g (91%). T_g = 77 °C (DSC). ^{1}H NMR (400 MHz, $CDCl_3$, δ, ppm): 8.47 (dd, 2H, J_1 = 13.4 Hz, J_2 = 1.4 Hz), 8.28 (d, 1H, J = 7.6 Hz), 8.23 (d, 1H, J = 7.6 Hz), 8.14 (d, 2H, J = 8.4 Hz), 7.97-7.94 (m, 2H), 7.88-7.81 (m, 4H), 7.69-7.65 (m, 2H), 7.62-7.57 (m, 3H), 7.55-7.46 (m, 4H), 7.39 (t, 1H, J = 7.4 Hz), 7.30 (t, 1H, J = 7.4 Hz), 4.38 (t, 2H, J = 7.2 Hz), 1.96 (qu, 2H, J = 7.2 Hz), 1.47-1.39 (m, 4H), 0.94 (t, 3H, J = 7.0 Hz). ^{13}C NMR (101 MHz, $CDCl_3$, δ, m.d.): 195.65, 141.80, 140.95, 140.71, 139.72, 139.29, 137.51, 135.95, 135.31, 132.86, 132.66, 131.96, 130.07, 128.49, 126.33, 126.20, 126.10, 125.78, 125.48, 124.50, 124.13, 123.46, 123.02, 120.69, 120.61, 120.48, 118.99, 118.84, 110.07, 109.94, 108.97, 108.85, 43.23, 29.49, 28.78, 22.54, 14.01. MS ($APCI^+$, 20 V): 582.34 ([M+H], 100%).

4-(9′-Hexyl-[3,3′]-bicarbazol-9-yl)benzophenone (DB38) was synthesized by stirring 9-hexyl-9′H-3,3′-bicarbazole (3) (0.50 g, 1.20 mmol) with 4-fluorobenzophenone (0.24 g, 1.20 mmol) in 10 ml of DMSO at 150 °C under an inert nitrogen atmosphere with potassium carbonate (1.66 g, 12.00 mmol) present. After 4 hours, TLC was used to confirm the completion of the reaction, following which the reaction mixture was slowly added to ice water. Chloroform was employed to extract the organic phase, and any remaining water traces in the organic phase were removed by adding anhydrous Na_2SO_4, which was filtered off later. The desired product was purified via column chromatography using tetrahydrofuran/hexane (volume ratio 1:7) as the mobile phase and silica gel as the stationary phase, resulting in yellow amorphous material with a yield of 0.67 g (94%). T_g = 68 °C (DSC). ^{1}H NMR (400 MHz, $CDCl_3$, δ, ppm): 8.48 (dd, 2H, J_1 = 12.4 Hz, J_2 = 1.6 Hz), 8.28 (d, 1H, 7.6 Hz), 8.23 (d, 1H, J = 8.0 Hz), 8.14 (d, 2H, J = 8.8 Hz), 7.97-7.95 (m, 2H), 7.88-7.81 (m, 4H), 7.69-7.65 (m, 2H), 7.62-7.58 (m, 3H), 7.56-7.45 (m, 4H), 7.39 (t, 1H, J = 7.2 Hz), 7.30 (t, 1H, J = 7.2 Hz), 4.38 (t, 2H, J = 7.2 Hz), 1.95 (qu, 2H, J = 7.4 Hz), 1.49-1.33 (m, 6H), 0.92 (t, 3H, J = 7.0 Hz). ^{13}C NMR (101 MHz, $CDCl_3$-d_6, δ, m.d.): 196.04, 141.80, 140.95, 140.70, 140.22, 139.01, 137.50, 135.95, 135.32, 132.86, 132.66, 131.97, 130.07, 128.55, 128.48, 127.24, 126.33, 126.21, 126.10, 125.77, 125.48, 124.49, 123.45, 123.01, 120.69, 120.62, 120.48, 119.00, 118.83, 110.07, 109.94, 108.97, 108.84, 43.26, 31.63, 29.03, 27.02, 22.60, 14.06. MS (APCI$^+$, 20 V): 596.36 ([M+H], 100%).

4-(9′-{2-Ethylhexyl}-[3,3′]-bicarbazol-9-yl)benzophenone (DB39) was synthesized by stirring 9-{2-ethylhexyl}-9′H-3,3′-bicarbazole (3) (0.50 g, 1.13 mmol) with 4-fluorobenzophenone (0.23 g, 1.13 mmol) in 10 ml of DMSO at 150 °C under an inert nitrogen atmosphere with potassium carbonate (1.56 g, 11.30 mmol) present. After 4 hours, TLC was used to confirm the completion of the reaction, following which the reaction mixture was slowly added to ice water. Chloroform was employed to extract the organic phase, and any remaining water traces in the organic phase were removed by adding anhydrous Na_2SO_4, which was filtered off later. The desired product was purified via column chromatography using tetrahydrofuran/hexane (volume ratio 1:7) as the mobile phase and silica gel as the stationary phase, resulting in pale-yellow amorphous material with a yield of 0.56 g (79%). T_g = 64 °C (DSC). ^{1}H NMR (400 MHz, $CDCl_3$, δ, ppm): 8.48 (dd, 2H, J_1 = 15.2 Hz, J_2 = 1.6 Hz), 8.28 (d, 1H, J = 7.6 Hz), 8.24 (d, 1H, J = 7.6 Hz), 8.14 (d, 2H, J = 8.8 Hz), 7.97-7.95 (m, 2H), 7.86-7.81 (m, 4H), 7.69-7.65 (m, 2H), 7.62-7.58 (m, 3H), 7.55-7.45 (m, 4H), 7.40 (t, 1H, J = 7.2 Hz), 7.30 (t, 1H, J = 8.0 Hz), 4.26-4.23 (m, 2H), 2.21-2.13 (m, 1H), 1.50-1.31 (m, 8H), 0.98 (t, 3H, J = 7.4 Hz), 0.93 (t, 3H, J = 7.2 Hz). ^{13}C NMR (101MHz, $CDCl_3$, δ, m.d.): 195.66, 141.81, 141.43, 140.71, 140.21, 139.29, 137.51, 135.94, 135.30, 132.82, 132.66, 131.97, 130.08, 128.50, 126.33, 126.20, 126.09, 125.75, 125.46, 124.51, 124.15, 123.42, 122.99, 120.70, 120.61, 120.43, 118.99, 118.92, 118.82, 110.08, 109.95, 109.27, 109.14, 47.57, 39.50, 31.07, 28.90, 24.46, 23.12, 14.11, 10.97. MS (APCI$^+$, 20 V): 624.44 ([M+H], 100%).

4-(9′-Octyl-[3,3′]-bicarbazol-9-yl)benzophenone (DB40) was synthesized by stirring 9-octyl-9′H-3,3′-bicarbazole (3) (0.50 g, 1.13 mmol) with 4-fluorobenzophenone (0.23 g, 1.13 mmol) in 10 ml of DMSO at 150 °C under an inert nitrogen atmosphere with potassium carbonate (1.56 g, 11.30 mmol) present. After 4 hours, TLC was used to confirm the completion of the reaction, following which the reaction mixture was slowly added to ice water. Chloroform was employed to extract the organic phase, and any remaining water traces in the organic phase were removed by adding anhydrous Na_2SO_4, which was filtered off later. The desired product was purified via column chromatography using tetrahydrofuran/hexane (volume ratio 1:7) as the mobile phase and silica gel as the stationary phase, resulting in pale-yellow amorphous material with a yield of 0.67 g (95%). T_g = 57 °C (DSC). ^{1}H NMR (400 MHz, $CDCl_3$, δ, ppm): 8.48 (dd, 2H, J_1 = 13.8 Hz, J_2 = 1.4 Hz), 8.28 (d, 1H, J = 7.6 Hz), 8.24 (d, 1H, J = 7.6 Hz), 8.14 (d, 2H, J = 8.4 Hz), 7.97-7.95 (m, 2H), 7.86-7.81 (m, 4H), 7.70-7.65 (m, 2H), 7.62-7.58 (m, 3H), 7.56-7.46 (m, 4H), 7.39 (t, 1H, J = 7.4 Hz), 7.30 (t, 1H, J = 7.6 Hz), 4.38 (t, 2H, J = 7.6 Hz), 1.95 (pent, 2H, J = 7.6 Hz), 1.48-1.29 (m, 10H), 0.91 (t, 3H, J = 7.4 Hz). ^{13}C NMR (101 MHz, $CDCl_3$, δ, m.d.): 195.66, 141.81, 140.96, 140.72, 139.72, 139.30, 137.51, 135.96, 135.33, 132.87, 132.65, 131.95, 130.07, 128.49, 126.32, 126.21, 126.10, 125.77, 125.48, 124.50, 124.14, 123.46, 123.02, 120.69, 120.60, 120.48, 119.00, 118.83, 110.06, 109.94, 108.97, 108.85, 43.26, 31.83, 29.43, 29.21, 29.06, 27.37, 22.63, 14.09. MS (APCI$^+$, 20 V): 624.44 ([M+H], 100%).

2.3. Fabrication and Characterization of Devices

A glass substrate with a pre-patterned indium tin oxide (ITO) layer was utilized in the production process of OLEDs. The mentioned substrate underwent a cleaning procedure firstly with acetone for 30 minutes at 50°C followed by a cleaning with isopropyl alcohol for 30 minutes at 60°C.

Subsequently, the cleaned substrates were exposed to UV radiation for 10 minutes in a preheated UV chamber. The layer deposition process took place within a glove box under an inert atmosphere. For the subsequent layer, the hole injecting material poly(3,4-ethylene-dioxythiophene):poly(styrenesulfonate) (PEDOT:PSS) was employed. It was spin-coated onto the substrate at 4000 rpm for 20 seconds, followed by heating the substrates for 10 minutes at 130°C. After cooling the substrates, the emissive layers, composed of host material and emitter, were formed on top of the hole injection layer. For deposition, spin-coating was also employed by spinning substrates for 20 seconds at 2500 rpm. Subsequently, the electron transporting layer, consisting of 1,3,5-tris(N-phenyl-benzimidazol-2-yl)benzene (TPBi), a LiF electron injecting layer, and aluminum cathode, were formed in a thermal evaporation chamber under a vacuum of 10^{-6} torr. Following this, the resulting devices, with an area of $0.09 cm^2$, were placed in a mini chamber within the glove box under vacuum until further tests were conducted. These tests were performed under normal atmospheric conditions in complete darkness. The CS-100A luminance and color meter was utilized to record voltage-current density and voltage-luminance characteristics. Additionally, the SpectraScan® spectroradiometer PR-655 was used to create luminance-power efficacy and luminance-current graphs. The measurements of current-voltage characteristics were conducted using a Keithley voltmeter. EQE was calculated using the method outlined in the literature [60].

3. Results and Discussions

3.1. Synthesis

Novel electroactive bicarbazole-based derivatives were synthesized via a three-step procedure illustrated in Scheme 1. Initially, 9H-carbazole underwent oxidation with iron(III) chloride to yield 9H,9′H-3,3′-bicarbazole (2). Subsequently, various alkyl bromides were utilized for the partial N-alkylation of 9H,9′H-3,3′-bicarbazole (2) in THF solution, resulting in the production of 9-alkyl-9′H-3,3′-bicarbazoles (3-8) in the presence of potassium hydroxide and potassium carbonate. Finally, the obtained bicarbazole derivatives (3-8) underwent nucleophilic substitution reactions with 4-fluorobenzophenone in DMSO in the presence of potassium carbonate, leading to the formation of the target derivatives DB37, DB38, DB39, DB40, DB41, and DB44. The chemical structures of these new electroactive compounds were confirmed using mass spectrometry and NMR spectroscopy, demonstrating excellent alignment with the theoretical structures. The aliphatic chains present in the synthesized target compounds contributed to increased solubility in commonly used organic solvents, consistent with the findings of Inoue et al. regarding the relationship between alkyl chain length and the solubility of organic materials [56]. The solubility of a material in an appropriate solvent is enhanced by extending the length of the alkyl chain. While the thermal evaporation method is suitable for producing thin layers for devices using these electroactive compounds, the good solubility of the new materials suggests a cost-effective alternative method for forming thin films through spin coating from a solution.

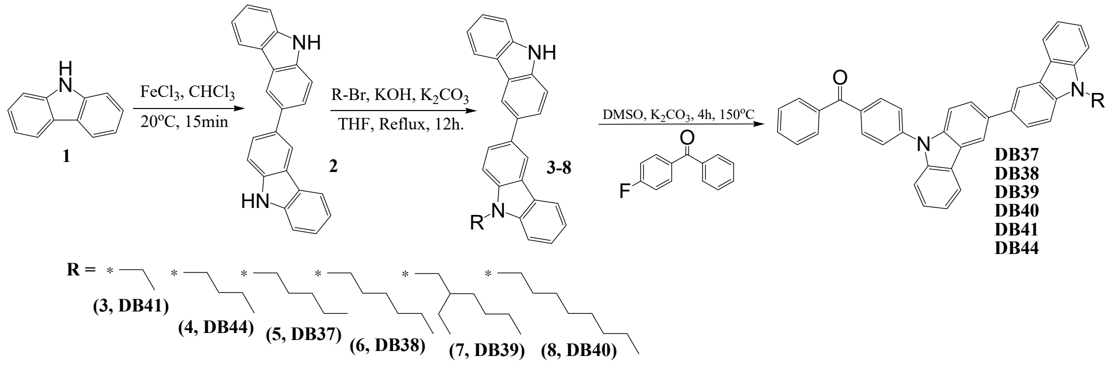

Scheme 1. Synthesis of target compounds DB37, DB38, DB39, DB40, DB41 and DB44.

3.2. Thermal and Morphological Properties

The response of the synthesized materials DB37-DB41 and DB44 to heating was investigated using DSC and TGA methods, heating the samples under an inert nitrogen atmosphere. Following TGA experiments conducted at a heating rate of 10 °C/min, it was observed that the target compounds exhibit remarkable stability under heating. As depicted in Figure 1, the TGA curve of compound DB37 illustrates a temperature of 5% weight loss (T_d) at 406 °C. Similarly, derivatives DB41 and DB44 demonstrated stability under heating, with respective T_d values of 374 °C and 389 °C. Materials DB38, DB39, and DB40, which feature longer aliphatic groups, exhibited comparable thermal stability, reaching T_d values of 398 °C, 383 °C, and 397 °C, respectively. The TGA curves for all investigated derivatives are provided in Figure S1 of the supplementary material for the publication.

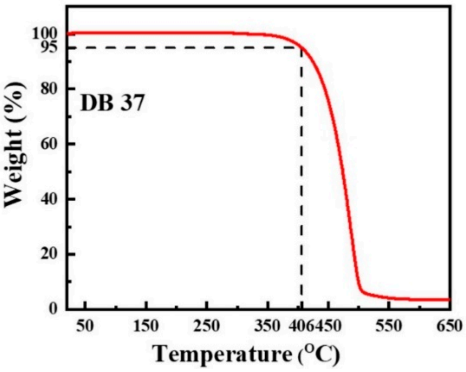

Figure 1. TGA curve of compound DB37.

Figure 2 displays the thermograms from DSC experiments conducted on all compounds DB37-DB41 and DB44. Upon examining the curves from the second heating, it becomes evident that the glass transition temperatures (Tg) are influenced by the length of their alkyl sidechains. For instance, material DB41, containing an ethyl group, exhibited a notably high Tg of 102 °C. Conversely, compounds DB44 and DB37, which are substituted with butyl and pentyl groups respectively, displayed slightly lower Tg values of 80 °C and 77 °C. This trend persists for materials featuring even longer alkyl groups: derivatives DB38, DB39, and DB40, substituted with hexyl, 2-ethylhexyl, and octyl groups respectively, exhibited glass transition temperatures of 68 °C, 64 °C, and 57 °C. In summary, the findings from TGA and DSC analyses affirm the suitability of these materials for use in the amorphous electroactive layers of OLED devices. Thermal characteristics are presented in Table 1 as well.

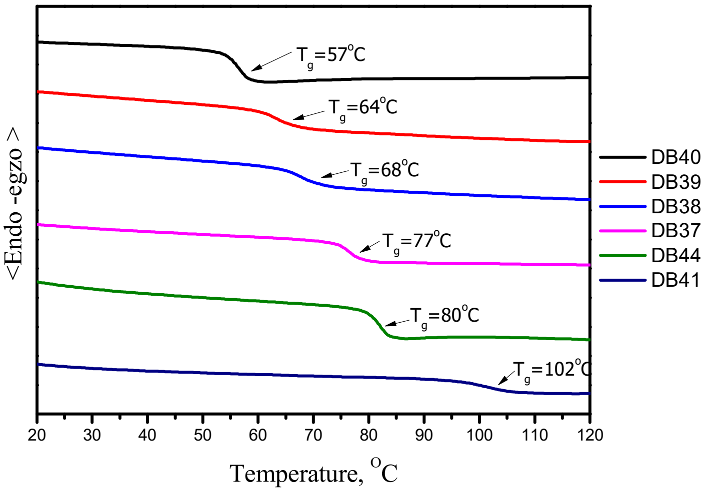

Figure 2. DSC thermo-grams from the second heating cycle of the target compounds.

Table 1. Characteristics of the derivatives DB37, DB38, DB39, DB40, DB41 and DB44.

Emitter	λ_{em} (nm)	λ_{em} (nm)	Φ (%)	Homo (eV)	Lumo (eV)	E_g (eV)	Decay (ns)	S_1 (eV)	T_1 (eV)	ΔE_{ST}	T_d (°C)	T_g (°C)
DB37	384.5, 395.6	509	65.5	-5.67	-2.58	3.09	5.53	3.04	2.76	0.28	406	102
DB38	383.5, 400	510	45.3	-5.70	-2.61	3.09	1.88	2.94	2.89	0.05	398	80
DB39	382.7, 400	528	75.5	-5.68	-2.60	3.08	4.27	3.10	2.81	0.29	383	77
DB40	384.5, 408.2	513	52.5	-5.69	-2.59	3.10	2.41	3.06	2.80	0.26	397	68
DB41	381.0, 399.7	528	62.5	-5.73	-2.64	3.09	2.24	3.22	2.80	0.42	374	64
DB44	383.9, 398.6	529	68.5	-5.69	-2.62	3.07	6.28	3.18	2.82	0.15	389	57

λ_{ex}: Excitation Wavelength; λ_{em}: Emission Wavelength; Φ: Photoluminescence Yield; E_g: Bandgap S_1 : Singlet Energy; T_1: Triplet Energy; ΔE_{ST} : Singlet-Triplet Energy Gap; T_d : Destruction temperature; T_g: Glass Transition Temperature.

3.3. Electrochemical and Photophysical Properties

The compounds DB37, DB38, DB39, DB40, DB41, and DB44 demonstrate elevated photoluminescence quantum yields (PLQY) of 65.5%, 45.3%, 75.5%, 52.5%, 62.5%, and 68.5%, respectively. Summarized values of PLQY can be found in Table 1. Figure 3 illustrates the UV-absorption bands of compound DB37 as an example. All the UV-absorption bands and Tauc plots for all the compounds are illustrated in Figure S2 of supplementary material of this article. The derivatives were examined in THF solvent under standard conditions using a quartz cuvette.

Notably, each of the derivatives consistently displayed two absorption peaks around 380 and 410 nm, attributed to the presence of identical chromophores within their structures. Tauc plots for objective compounds were generated by employing The UV absorption wavelength and intensity, using equations $(\alpha \times h\nu)^{1/2}$ and hν for the x-axis and y-axis, respectively, where α denotes intensity and hν stands for energy (hν = 1240/wavelength). The Tauc plots unveiled bandgaps for the studied derivatives: DB37, DB38, and DB41 had a bandgap of 3.09 eV, DB40 had a bandgap of 3.10 eV, DB39 had a bandgap of 3.08 eV, and DB44 had a bandgap of 3.07 eV (see Table 1).

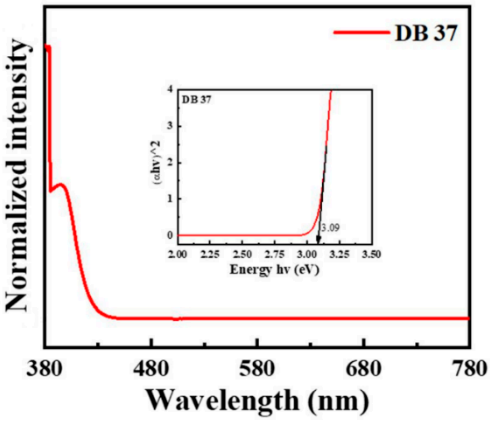

Figure 3. UV-Vis absorbance spectrum and tauc plot (inset) of the compound **DB37**.

Figure 4 illustrates the evaluation of electrochemical characteristics of DB37, DB38, DB39, DB40, DB41, and DB44 through CV measurements. Obtained oxidation onset values were used for calculations of HOMO levels, employing equation E$_{HOMO}$ = -[4.4 + E_{onset}^{ox}], while the determination of LUMO levels was accomplished using equation E$_{LUMO}$ = E$_{HOMO}$ + E$_g$ following the methodology described in the literature [18,61,62]. The determined HOMO levels for DB37, DB38, DB39, DB40, DB41, and DB44 were -5.67, -5.70, -5.68, -5.69, -5.73, and -5.69, respectively. Meanwhile, LUMO levels were, in the same order, -2.58, -2.61, -2.60, -2.59, -2.64, and -2.62. These values along with E$_g$ levels are outlined in Table 1. HOMO and LUMO levels of the compounds are appropriate to forming blue-emitting layers in tandem with the commercial host material CBP.

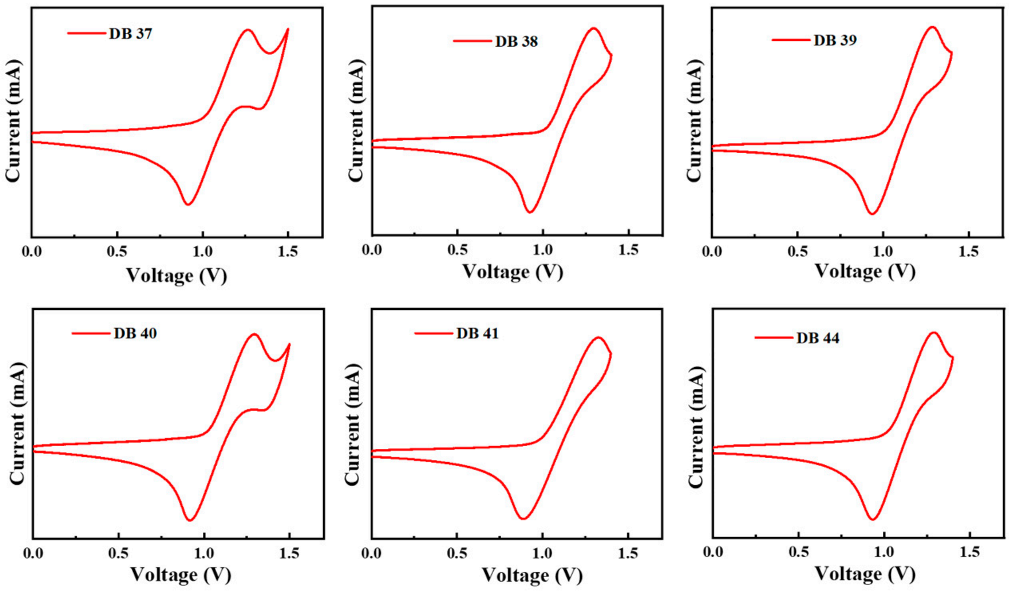

Figure 4. Curves of CV scans of the materials DB37, DB38, DB39, DB40, DB41, and DB44.

In Figure 5 (left) as an example, the PL spectrum of DB37 compound is presented, displaying emission wavelength maximum at about 510 nm with cyan blue emission. Singlet state energies of the potential emitters were calculated by utilizing the crossing point of PL and absorbance charts, resulting in values of 3.04 eV for DB37, 2.94 eV for DB38, 3.10 eV for DB39, 3.06 eV for DB40, 3.22 eV for DB41, and 3.18 eV for DB44 (see Table 1).

Additionally, low-temperature photoluminescence (LTPL) spectra were registered to ascertain the triplet energy levels. The spectrum for DB37 is depicted in Figure 5 (right) as an example. The compounds DB37, DB38, DB39, DB40, DB41, and DB44 demonstrate elevated levels of triplet energy at 2.76, 2.89, 2.81, 2.80, 2.80, and 2.82 eV, respectively, suggesting their potential suitability as blue emitters. The LTPL spectra of all the objective derivatives are presented in Figure S3 of supplementary material, and the triplet state energy values are listed in Table 1.

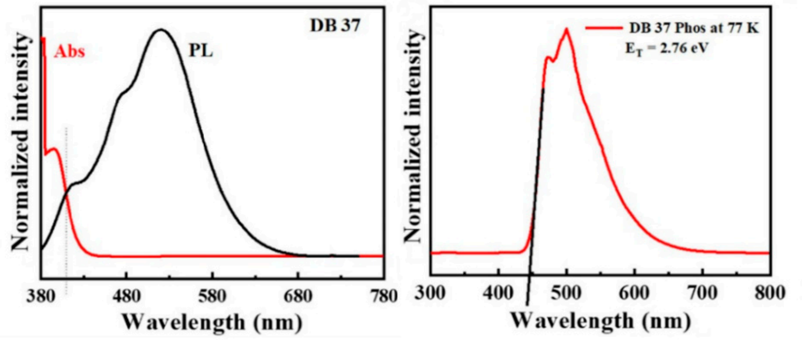

Figure 5. Photoluminescence (left) and low-temperature photoluminescence (right) spectra of the material **DB37**.

Figure 6 displays the results of the time-resolved photoluminescence (TRPL) experiments illustrating decay times of photoluminescence for the new emitters. The determined values of the time for DB37, DB38, DB39, DB40, DB41, and DB44 was 5.53, 1.88, 4.27, 2.41, 2.24, and 6.28 ns, respectively. Typically, the decay lifetime of fluorescent emitters falls within the picosecond range. However, the presented materials exhibit decay on the nanosecond scale, suggesting potential utilization of triplet excited states. The photoluminescence decay times are detailed in Table 1. In the graphs, IRF denotes the instrument response function, which was measured both prior to and following each measurement as a control parameter.

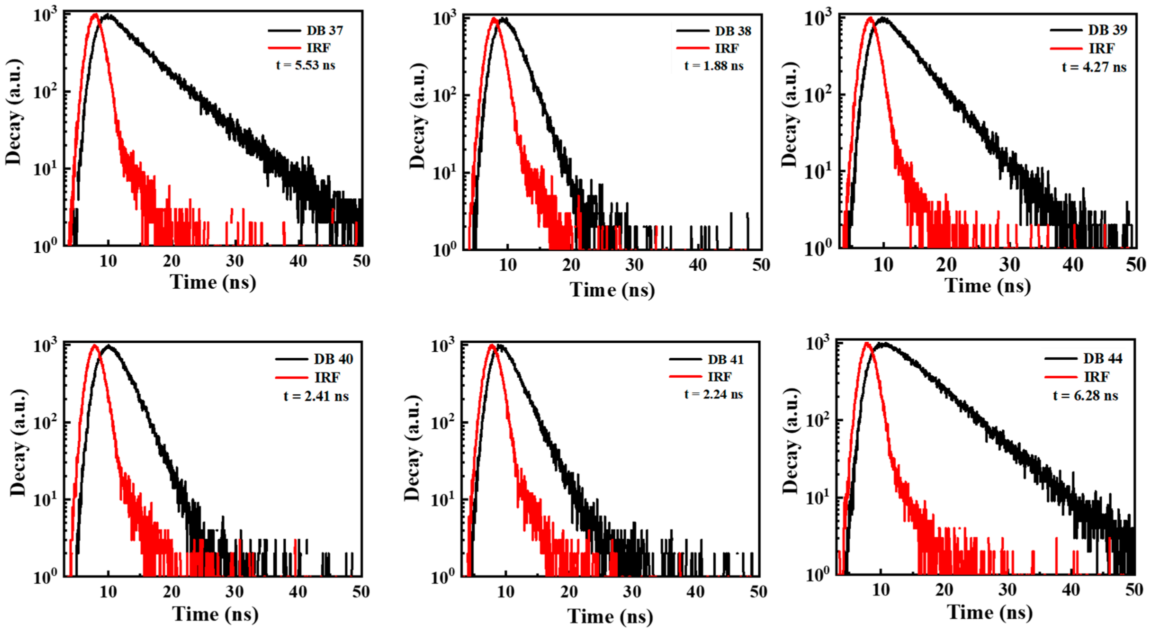

Figure 6. TRPL spectra of the compounds DB37, DB38, DB39, DB40, DB41, and DB44.

3.4. Electroluminescent Properties

The OLED devices architecture utilized in this study is represented by the energy level diagram depicted in Figure 7. These devices incorporate emitters DB37, DB38, DB39, DB40, DB41, and DB44 doped in a CBP host material. The straightforward device structures consisted of a 125 nm ITO anode layer, followed by a 35 nm PEDOT:PSS hole injection layer (HIL), and subsequently a 30 nm emissive layer (EML) comprising a CBP host with dopants DB37, DB38, DB39, DB40, DB41, or DB44 (at concentrations of 5%, 10%, 15%, and 100% by weight). As for the electron transporting layer (ETL), 1,3,5-Tris(N-phenyl-benzimidazol-2-yl)benzene (TPBi, 32 nm) was employed, while lithium fluoride (LiF, 0.8 nm) served as the electron injecting layer (EIL), and aluminum (Al, 150 nm) was used as the cathode layer.

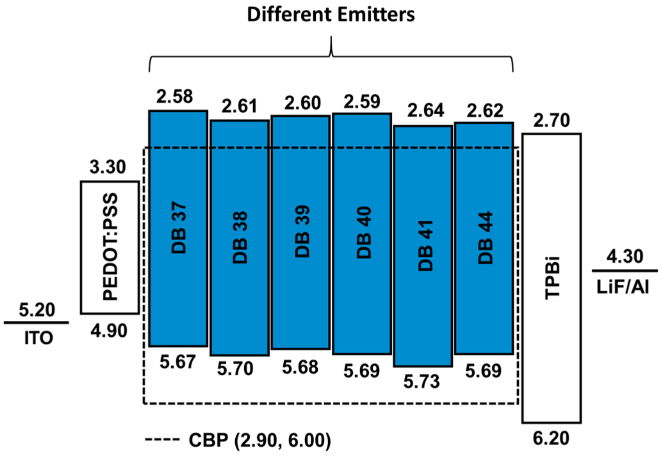

Figure 7. Energy-level diagram of the OLEDs employing the emitters DB37, DB38, DB39, DB40, DB41 and DB44 doped in CBP host.

All new objective compounds, owing to their solubility were suitable for layer preparation through spin-coating and were examined as emitters dispersed in a CBP host for the OLEDs. All of new emissive materials underwent concentration-dependent experiments with proportions of 5, 10, 15, or 100 wt% of each guest in the emissive layer. The electroluminescence (EL) properties, like power efficacy (PE), current efficacy (CE), EQE, maximum luminance (L_{MAX}) and the International Commission on Illumination (CIE) colour space coordinates of the devices utilizing the newly introduced emitting materials distributed within the CBP host, along with the respective non-doped devices, are outlined in Table 2. Furthermore, Figure 7 visually represents the EL characteristics of devices employing the most efficient emitter DB39. The Figure illustrates EL spectra of the devices, current density-voltage-luminance and power efficacy-luminance-current efficact characteristics. The same characteristics of OLEDs using other emitters DB37, DB38, DB40, DB41, and DB44 are depicted in Figures S4, S5, S6, S7, and S8 in the supplementary material of this article, respectively.

Table 2. EL characteristics of the OLEDs containing emitting materials DB37, DB38, DB39, DB40, DB41 and DB44.

Emitter	Concentration (wt%)	Turn-on Voltage (V_{on})^a	Power efficacy (lm/W)	Current efficacy (cd/A)	EQE (%)	CIE_{xy}	L_{Max} (cd/m^2)
			@100 cd/m²/@1,000 cd/m²/max			@100cd/m² / @1000cd/m²	
DB37	**5.0**	**4.0**	**2.1/1.1/3.4**	**3.4/2.4/3.9**	2.1/1.6/2.1	(0.17, 0.22) / (0.17, 0.30)	3449
	10	3.5	2.5/1.3/3.4	3.5/2.5/3.8	1.8/1.5/1.9	(0.18, 0.26) / (0.18, 0.23)	3658
	15	3.4	2.8/1.5/3.6	3.7/2.7/4.0	1.7/1.5/1.8	(0.19, 0.28) / (0.18, 0.25)	3464
	100	3.1	0.3/ - / -	0.3/ - / -	0.1 / - / -	(0.24, 0.40) / -	616
DB38	5.0	3.9	1.9/1.0/3.4	3.1/2.2/3.8	1.9/1.5/1.9	(0.18, 0.22) / (0.17, 0.20)	2801
	10	3.5	2.7/1.4/2.9	3.7/2.7/3.8	2.0/1.6/1.9	(0.18, 0.25) / (0.18, 0.22)	3430
	15	3.4	2.8/1.5/3.5	3.6/2.8/4.2	1.7/1.6/1.8	(0.19, 0.27) / (0.18, 0.24)	3555
	100	3.2	0.2/ - / -	0.3/ - / -	0.1/ - / -	(0.22, 0.38) / -	618
DB39	5.0	4.0	1.8/0.9/3.3	3.1/2.2/3.7	2.0/1.6/2.1	(0.18, 0.20) / (0.17, 0.18)	2818
	10	3.5	2.5/1.3/4.4	3.5/2.7/4.9	2.0/1.8/2.2	(0.18, 0.23) / (0.18, 0.21)	3430
	15	**3.9**	**3.0/1.4/4.1**	**4.4/2.8/5.7**	**2.2/1.6/2.7**	(0.19, 0.27) / (0.19, 0.24)	**3581**
	100	3.4	0.3/ - / -	0.4/ - / -	0.4/ - / -	(0.24, 0.39) / -	615
DB40	5.0	4.2	2.0/1.1/2.1	3.4/2.4/3.4	2.2/1.6/2.3	(0.17, 0.22) / (0.17, 0.20)	3166
	10	3.5	2.8/1.5/2.9	3.8/2.8/3.7	2.0/1.7/2.0	(0.18, 0.25) / (0.18, 0.22)	3840
	15	3.3	2.8/1.6/2/8	3.6/2.8/3.6	1.8/1.6/1.8	(0.18, 0.27) / (0.18, 0.24)	3950
	100	3.2	0.2/ - / -	0.3/ - / -	0.1 / - / -	(0.22, 0.38) / -	685
DB41	5.0	4.4	1.6/0.8/1.9	2.9/1.9/3.1	1.9/1.3/2.0	(0.18, 0.21) / (0.18, 0.19)	2687
	10	3.8	2.4/1.1/2.4	3.6/2.5/3.6	2.0/1.5/2.0	(0.19, 0.26) / (0.19, 0.23)	3347
	15	3.5	2.6/1.3/2.7	3.6/2.5/3.6	1.7/1.1/1.8	(0.20, 0.28) / (0.19, 0.24)	3128
	100	3.1	0.2/ - / -	0.3/ - / -	0.1/ - / -	(0.30, 0.45) / -	486
DB44	5.0	4.8	1.6/0.7/1.6	3.3/2.2/3.3	2.3/ - /2.3	(0.17, 0.20) / -	1718
	10	4.0	2.1/0.8/2.7	3.9/2.3/4.1	2.1/1.4/2.3	(0.18, 0.24) / (0.18, 0.22)	1283
	15	3.8	2.1/0.5/2.3	3.6/1.5/3.7	1.9/ - /2.0	(0.19, 0.26) / -	1275
	100	5.1	- / - / -	- / - / -	- / - / -	- / -	55

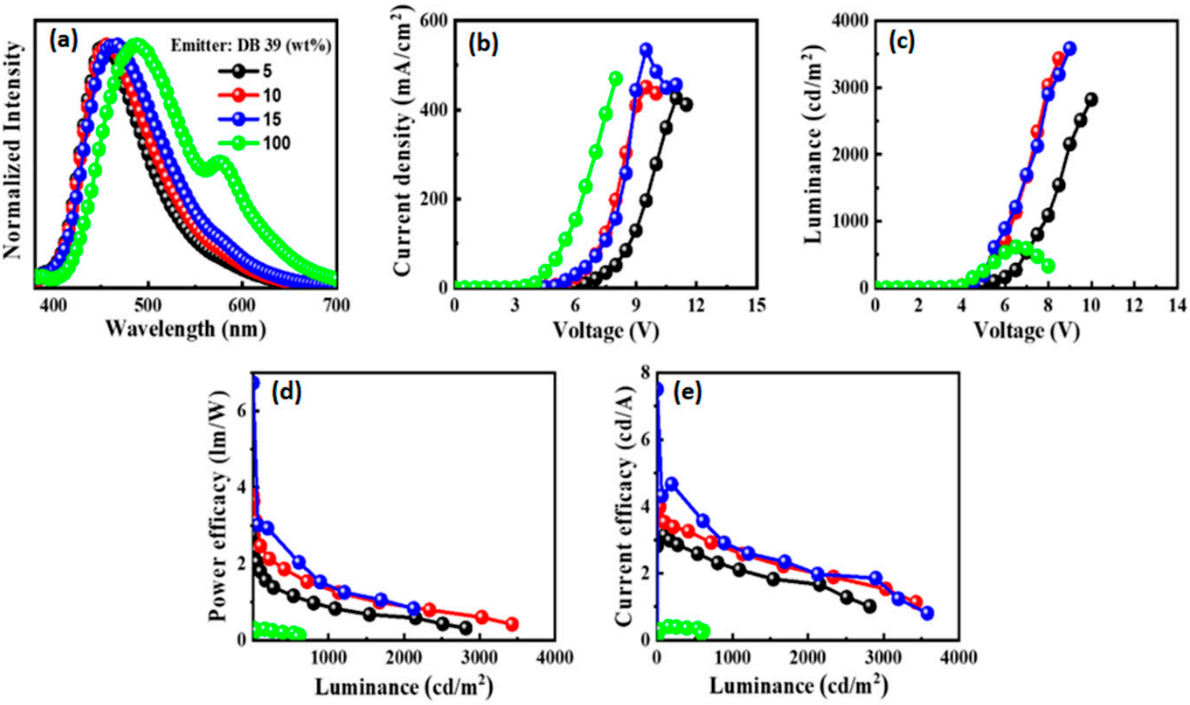

Figure 7. The EL characteristics of the device, whether with pure emitter DB39 or doped within a CBP host material at different concentrations, are depicted, illustrating EL spectra (a), current density–voltage (b), luminance–voltage (c), power efficiency–luminance (d), and current efficiency–luminance (e) characteristics.

In Figure 7(a), the EL spectra of devices incorporating the DB39 dopant demonstrate peaks within the 460-490 nm range, indicating emission in blue region. The presence of distinct peaks implies effective energy transfer from the host to the guest. Evidently, both undoped and doped OLEDs demonstrate comparable EL emission peaks. Figures 7(b-e) illustrate the characteristics of current density-luminance-voltage and power efficiency-luminance-current efficiency. Although the undoped device exhibits a higher current density than the doped devices, it notably demonstrates lower efficiency than the doped devices, highlighting the significant influence of the host material. As depicted in Table 2, the OLED based on DB39 displays the best efficiencies out of all these devices. This enhanced performance can be ascribed to the inclusion of the elongated and branched 2-ethylhexyl sidechain in the molecule, potentially improving solubility for production of wet-processed OLEDs and contributing to favorable film-forming characteristics of the derivative. Moreover, appropriate HOMO and LUMO levels facilitate effective energy transfer from host to, while the combination of the electron-accepting benzophenone functional group with the bicarbazole donor moiety promotes balanced charge transfer, boosting performance even more. Specifically, the device containing 10 wt% of emitter DB39 demonstrates the highest PE of 4.4 lm/W, with a L_{MAX} reaching 3430 cd/m^2. However, the overall best efficiency is achieved by the device incorporating 15wt% of emitter DB39 in its emissive layer, attaining PE and CE values of 4.1 lm/W and 5.7 cd/A, respectively, shile EQE reached 2.7%, with L_{MAX} reaching 3581 cd/m^2.

4. Conclusions

We introduced novel emissive derivatives synthesized through a three-step process, utilizing bicarbazole and benzophenone as building blocks to achieve twisted donor-acceptor structures. The incorporation of alkyl sidechains of varying length was chosen to Enhance the solubility and film-forming characteristics of the materials. Newly synthesized derivatives exhibited commendable thermal and morphological stability, evidenced by elevated temperatures of 5% mass loss ranging from 374 °C to 406 °C. The manipulation of alkyl sidechain length allowed control over glass-transition temperatures that spanned from 57 °C to desirable 102 °C. Additionally, newly developed materials demonstrated short decay times, confirmed by time-resolved photoluminescence, and high photoluminescence quantum yields of up to 75.5%. The benzophenone-based derivatives exhibited favourable HOMO-LUMO levels, as well as triplet-singlet state energy values suitable for applications as blue emitters. Upon investigation electroluminescent properties of the new devices, an OLED with emissive layer comprising from 15 wt% DB39 doped in CBP host surpassed other devices in terms of efficiencies. The maximum current efficacy (CE_{max}) reaching 5.7 cd/A and 2.7% external quantum efficacy (EQE_{max}) were detected followed by maximum luminance (L_{max}) of 3,581 cd/m^2 with a turn-on voltage of 3.9 V. This study emphasized the notable influence of energy transfer from host to guest, ideal doping concentrations, also the effect of chemical structure on solubility, thereby impacting the efficiency of wet-processed devices. It's crucial to highlight that these characteristics were observed in non-optimized OLEDs using standard laboratory conditions, suggesting potential enhancements through optimization processes. Furthermore, enhancing of devices efficiency could be achieved by reducing ΔE_{ST} and effectively utilizing triplet-state excitons of similar materials, making them suitable for highly efficient lighting applications. We believe that our findings suggest the potential of some materials for further exploration as promising emitters.

Supplementary Materials: The following can be accessed online: Figure S1: TGA curves of materials DB37, DB38, DB39, DB40, DB41 and DB44, Figure S2: UV-Vis absorption bands and Tauc plots of materials DB37, DB38, DB39, DB40, DB41 and DB44, Figure S3: singlet energy calculation of the compounds DB37 – DB41 and DB44 using the crossing of PL and absorbance graphs, Figure S4: LTPL spectra at 77K and triplet energy calculation of the derivatives DB37, DB38, DB39, DB40, DB41 and DB44, Figures S5, S6, S7, S8 and S9: The electroluminescent (EL) characteristics of OLEDs with dopants DB37, DB38, DB40, DB41 and DB44, respectively, doped within a CBP host matrix at different concentrations, displaying EL spectra, current density–voltage, luminance–voltage, power efficacy–luminance, and current efficacy–luminance dependencies.

Author Contributions: Investigation, I.S., P.G., J.J., S.L., D.B., D.T. and E.Z.; writing—original draft preparation, I.S., P.G. and D.B.; writing—review and editing, S.G. and J.-H.J. All authors have read and agreed to the published version of the manuscript.

Funding: This work was supported by the Ministry of Science and Technology (MOST), Taiwan (Grant No. 109-2923-M-007-003-MY3) and by the project funded by the Research Council of Lithuania (Grant No. S-LLT-19-2).

Conflicts of interest: The authors declare no conflict of interest.

Sample Availability: Samples are not available from the authors.

References

1. Hong, G.; Gan, X.; Leonhardt, C.; Zhang, Z.; Seibert, J.; Busch, J.M.; Bräse, S. A Brief History of OLEDs—Emitter Development and Industry Milestones. *Advanced Materials* **2021**, *33*, doi:10.1002/adma.202005630.
2. Luo, Y.-J.; Lu, Z.-Y.; Huang, Y. Triplet Fusion Delayed Fluorescence Materials for OLEDs. *Chinese Chemical Letters* **2016**, *27*, 1223–1230, doi:10.1016/j.cclet.2016.06.002.
3. Zeng, H.; Huang, Q.; Liu, J.; Huang, Y.; Zhou, J.; Zhao, S.; Lu, Z. A Red-Emissive Sextuple Hydrogen-Bonding Self-Assembly Molecular Duplex Bearing Perylene Diimide Fluorophores for Warm-White Organic Light-Emitting Diode Application. *Chin J Chem* **2016**, *34*, 387–396, doi:10.1002/cjoc.201500771.
4. Zhang, Z.; Li, W.; Ye, K.; Zhang, H. Synthesis, Structure and Properties of a Novel Benzothiazole-Based Diboron-Bridged π-Conjugated Ladder. *Acta Chimi Sin* **2016**, *74*, 179, doi:10.6023/A15090603.
5. Yu, Y.; Yang, J.; Ren, Z.; Xie, G.; Li, Q.; Li, Z. Synthesis of Solution Processable Blue AIEgens and the Device Performance. *Acta Chimi Sin* **2016**, *74*, 865, doi:10.6023/A16070372.
6. Im, Y.; Byun, S.Y.; Kim, J.H.; Lee, D.R.; Oh, C.S.; Yook, K.S.; Lee, J.Y. Recent Progress in High-Efficiency Blue-Light-Emitting Materials for Organic Light-Emitting Diodes. *Adv Funct Mater* **2017**, *27*, doi:10.1002/adfm.201603007.
7. Root, S.E.; Savagatrup, S.; Printz, A.D.; Rodriquez, D.; Lipomi, D.J. Mechanical Properties of Organic Semiconductors for Stretchable, Highly Flexible, and Mechanically Robust Electronics. *Chem Rev* **2017**, *117*, 6467–6499, doi:10.1021/acs.chemrev.7b00003.

8. Kim, J.-J.; Han, M.-K.; Noh, Y.-Y. Flexible OLEDs and Organic Electronics. *Semicond Sci Technol* **2011**, *26*, 030301, doi:10.1088/0268-1242/26/3/030301.
9. Jeong, E.G.; Kwon, J.H.; Kang, K.S.; Jeong, S.Y.; Choi, K.C. A Review of Highly Reliable Flexible Encapsulation Technologies towards Rollable and Foldable OLEDs. *Journal of Information Display* **2020**, *21*, 19–32, doi:10.1080/15980316.2019.1688694.
10. Reineke, S.; Lindner, F.; Schwartz, G.; Seidler, N.; Walzer, K.; Lüssem, B.; Leo, K. White Organic Light-Emitting Diodes with Fluorescent Tube Efficiency. *Nature* **2009**, *459*, 234–238, doi:10.1038/nature08003.
11. Sun, Y.; Giebink, N.C.; Kanno, H.; Ma, B.; Thompson, M.E.; Forrest, S.R. Management of Singlet and Triplet Excitons for Efficient White Organic Light-Emitting Devices. *Nature* **2006**, *440*, 908–912, doi:10.1038/nature04645.
12. Wang, J.; Liang, J.; Xu, Y.; Liang, B.; Wei, J.; Li, C.; Mu, X.; Ye, K.; Wang, Y. Purely Organic Phosphorescence Emitter-Based Efficient Electroluminescence Devices. *J Phys Chem Lett* **2019**, *10*, 5983–5988, doi:10.1021/acs.jpclett.9b02513.
13. Yang, X.; Yue, L.; Yu, Y.; Liu, B.; Dang, J.; Sun, Y.; Zhou, G.; Wu, Z.; Wong, W. Strategically Formulating Aggregation-Induced Emission-Active Phosphorescent Emitters by Restricting the Coordination Skeletal Deformation of Pt(II) Complexes Containing Two Independent Monodentate Ligands. *Adv Opt Mater* **2020**, *8*, doi:10.1002/adom.202000079.
14. Rajamalli, P.; Senthilkumar, N.; Huang, P.-Y.; Ren-Wu, C.-C.; Lin, H.-W.; Cheng, C.-H. New Molecular Design Concurrently Providing Superior Pure Blue, Thermally Activated Delayed Fluorescence and Optical Out-Coupling Efficiencies. *J Am Chem Soc* **2017**, *139*, 10948–10951, doi:10.1021/jacs.7b03848.
15. Zhu, M.; Yang, C. Blue Fluorescent Emitters: Design Tactics and Applications in Organic Light-Emitting Diodes. *Chem Soc Rev* **2013**, *42*, 4963, doi:10.1039/c3cs35440g.
16. Du, C.; Lu, T.; Cheng, Z.; Chang, Y.; Liu, H.; Wang, J.; Wan, L.; Lv, Y.; Lu, P. Rational Molecular Design of Phenanthroimidazole-Based Fluorescent Materials towards High-Efficiency Non-Doped Deep Blue OLEDs. *J Mater Chem C Mater* **2022**, *10*, 14186–14193, doi:10.1039/D2TC02329F.
17. Xu, H.; Chen, R.; Sun, Q.; Lai, W.; Su, Q.; Huang, W.; Liu, X. Recent Progress in Metal–Organic Complexes for Optoelectronic Applications. *Chem. Soc. Rev.* **2014**, *43*, 3259–3302, doi:10.1039/C3CS60449G.
18. de Leeuw, D.M.; Simenon, M.M.J.; Brown, A.R.; Einerhand, R.E.F. Stability of N-Type Doped Conducting Polymers and Consequences for Polymeric Microelectronic Devices. *Synth Met* **1997**, *87*, 53–59, doi:10.1016/S0379-6779(97)80097-5.
19. Scholz, S.; Kondakov, D.; Lüssem, B.; Leo, K. Degradation Mechanisms and Reactions in Organic Light-Emitting Devices. *Chem Rev* **2015**, *115*, 8449–8503, doi:10.1021/cr400704v.
20. Lee, J.; Jeong, C.; Batagoda, T.; Coburn, C.; Thompson, M.E.; Forrest, S.R. Hot Excited State Management for Long-Lived Blue Phosphorescent Organic Light-Emitting Diodes. *Nat Commun* **2017**, *8*, 15566, doi:10.1038/ncomms15566.
21. Xing, L.; Zhu, Z.-L.; He, J.; Qiu, Z.; Yang, Z.; Lin, D.; Chen, W.-C.; Yang, Q.; Ji, S.; Huo, Y.; et al. Anthracene-Based Fluorescent Emitters toward Superior-Efficiency Nondoped TTA-OLEDs with Deep Blue Emission and Low Efficiency Roll-Off. *Chemical Engineering Journal* **2021**, *421*, 127748, doi:10.1016/j.cej.2020.127748.
22. Chen, J.; Tao, W.; Chen, W.; Xiao, Y.; Wang, K.; Cao, C.; Yu, J.; Li, S.; Geng, F.; Adachi, C.; et al. Red/Near-Infrared Thermally Activated Delayed Fluorescence OLEDs with Near 100 % Internal Quantum Efficiency. *Angewandte Chemie International Edition* **2019**, *58*, 14660–14665, doi:10.1002/anie.201906575.
23. Albrecht, K.; Matsuoka, K.; Fujita, K.; Yamamoto, K. Carbazole Dendrimers as Solution-Processable Thermally Activated Delayed-Fluorescence Materials. *Angewandte Chemie International Edition* **2015**, *54*, 5677–5682, doi:10.1002/anie.201500203.
24. Zhang, Q.; Li, J.; Shizu, K.; Huang, S.; Hirata, S.; Miyazaki, H.; Adachi, C. Design of Efficient Thermally Activated Delayed Fluorescence Materials for Pure Blue Organic Light Emitting Diodes. *J Am Chem Soc* **2012**, *134*, 14706–14709, doi:10.1021/ja306538w.
25. Wu, K.; Zhang, T.; Wang, Z.; Wang, L.; Zhan, L.; Gong, S.; Zhong, C.; Lu, Z.-H.; Zhang, S.; Yang, C. De Novo Design of Excited-State Intramolecular Proton Transfer Emitters via a Thermally Activated Delayed Fluorescence Channel. *J Am Chem Soc* **2018**, *140*, 8877–8886, doi:10.1021/jacs.8b04795.
26. Goushi, K.; Yoshida, K.; Sato, K.; Adachi, C. Organic Light-Emitting Diodes Employing Efficient Reverse Intersystem Crossing for Triplet-to-Singlet State Conversion. *Nat Photonics* **2012**, *6*, 253–258, doi:10.1038/nphoton.2012.31.

27. Ahn, D.H.; Kim, S.W.; Lee, H.; Ko, I.J.; Karthik, D.; Lee, J.Y.; Kwon, J.H. Highly Efficient Blue Thermally Activated Delayed Fluorescence Emitters Based on Symmetrical and Rigid Oxygen-Bridged Boron Acceptors. *Nat Photonics* **2019**, *13*, 540–546, doi:10.1038/s41566-019-0415-5.
28. Uoyama, H.; Goushi, K.; Shizu, K.; Nomura, H.; Adachi, C. Highly Efficient Organic Light-Emitting Diodes from Delayed Fluorescence. *Nature* **2012**, *492*, 234–238, doi:10.1038/nature11687.
29. Wang, Z.; Li, Y.; Cai, X.; Chen, D.; Xie, G.; Liu, K.; Wu, Y.-C.; Lo, C.-C.; Lien, A.; Cao, Y.; et al. Structure–Performance Investigation of Thioxanthone Derivatives for Developing Color Tunable Highly Efficient Thermally Activated Delayed Fluorescence Emitters. *ACS Appl Mater Interfaces* **2016**, *8*, 8627–8636, doi:10.1021/acsami.5b12559.
30. Im, Y.; Kim, M.; Cho, Y.J.; Seo, J.-A.; Yook, K.S.; Lee, J.Y. Molecular Design Strategy of Organic Thermally Activated Delayed Fluorescence Emitters. *Chemistry of Materials* **2017**, *29*, 1946–1963, doi:10.1021/acs.chemmater.6b05324.
31. Cai, X.; Li, X.; Xie, G.; He, Z.; Gao, K.; Liu, K.; Chen, D.; Cao, Y.; Su, S.-J. "Rate-Limited Effect" of Reverse Intersystem Crossing Process: The Key for Tuning Thermally Activated Delayed Fluorescence Lifetime and Efficiency Roll-off of Organic Light Emitting Diodes. *Chem Sci* **2016**, *7*, 4264–4275, doi:10.1039/C6SC00542J.
32. Hatakeyama, T.; Shiren, K.; Nakajima, K.; Nomura, S.; Nakatsuka, S.; Kinoshita, K.; Ni, J.; Ono, Y.; Ikuta, T. Ultrapure Blue Thermally Activated Delayed Fluorescence Molecules: Efficient HOMO–LUMO Separation by the Multiple Resonance Effect. *Advanced Materials* **2016**, *28*, 2777–2781, doi:10.1002/adma.201505491.
33. Zheng, X.; Huang, R.; Zhong, C.; Xie, G.; Ning, W.; Huang, M.; Ni, F.; Dias, F.B.; Yang, C. Achieving 21% External Quantum Efficiency for Nondoped Solution-Processed Sky-Blue Thermally Activated Delayed Fluorescence OLEDs by Means of Multi-(Donor/Acceptor) Emitter with Through-Space/-Bond Charge Transfer. *Advanced Science* **2020**, *7*, doi:10.1002/advs.201902087.
34. Ma, F.; Ji, H.; Zhang, D.; Xue, K.; Zhang, P.; Qi, Z.; Zhu, H. Adjusting the Photophysical Properties of AIE-Active TADF Emitters from through-Bond to through-Space Charge Transfer for High-Performance Solution-Processed OLEDs. *Dyes and Pigments* **2021**, *188*, 109208, doi:10.1016/j.dyepig.2021.109208.
35. Rajamalli, P.; Rota Martir, D.; Zysman-Colman, E. Pyridine-Functionalized Carbazole Donor and Benzophenone Acceptor Design for Thermally Activated Delayed Fluorescence Emitters in Blue Organic Light-Emitting Diodes. *J Photonics Energy* **2018**, *8*, 1, doi:10.1117/1.JPE.8.032106.
36. Ma, M.; Li, J.; Liu, D.; Li, D.; Dong, R.; Mei, Y. Low Efficiency Roll-off Thermally Activated Delayed Fluorescence Emitters for Non-Doped OLEDs: Substitution Effect of Thioether and Sulfone Groups. *Dyes and Pigments* **2021**, *194*, 109649, doi:10.1016/j.dyepig.2021.109649.
37. Wu, L.; Wang, K.; Wang, C.; Fan, X.-C.; Shi, Y.-Z.; Zhang, X.; Zhang, S.-L.; Ye, J.; Zheng, C.-J.; Li, Y.-Q.; et al. Using Fluorene to Lock Electronically Active Moieties in Thermally Activated Delayed Fluorescence Emitters for High-Performance Non-Doped Organic Light-Emitting Diodes with Suppressed Roll-Off. *Chem Sci* **2021**, *12*, 1495–1502, doi:10.1039/D0SC05631F.
38. Aizawa, N.; Tsou, C.-J.; Park, I.S.; Yasuda, T. Aggregation-Induced Delayed Fluorescence from Phenothiazine-Containing Donor–Acceptor Molecules for High-Efficiency Non-Doped Organic Light-Emitting Diodes. *Polym J* **2017**, *49*, 197–202, doi:10.1038/pj.2016.82.
39. Jing, Y.-Y.; Tao, X.-D.; Yang, M.-X.; Chen, X.-L.; Lu, C.-Z. Triptycene-Imbedded Thermally Activated Delayed Fluorescence Emitters with Excellent Film Morphologies for Applications in Efficient Nondoped and Doped Organic Light-Emitting Devices. *Chemical Engineering Journal* **2021**, *413*, 127418, doi:10.1016/j.cej.2020.127418.
40. Tani, K.; Yashima, T.; Miyanaga, K.; Hori, K.; Goto, K.; Tani, F.; Habuka, Y.; Suzuki, K.; Shizu, K.; Kaji, H. Carbazole and Benzophenone Based Twisted Donor–Acceptor Systems as Solution Processable Green Thermally Activated Delayed Fluorescence Organic Light Emitters. *Chem Lett* **2018**, *47*, 1236–1239, doi:10.1246/cl.180438.
41. Liu, Y.; Wu, X.; Chen, Y.; Chen, L.; Li, H.; Wang, W.; Wang, S.; Tian, H.; Tong, H.; Wang, L. Triazatruxene-Based Thermally Activated Delayed Fluorescence Small Molecules with Aggregation-Induced Emission Properties for Solution-Processable Nondoped OLEDs with Low Efficiency Roll-Off. *J Mater Chem C Mater* **2019**, *7*, 9719–9725, doi:10.1039/C9TC02927C.
42. Wang, J.; Zhang, J.; Jiang, C.; Yao, C.; Xi, X. Effective Design Strategy for Aggregation-Induced Emission and Thermally Activated Delayed Fluorescence Emitters Achieving 18% External Quantum Efficiency Pure-Blue OLEDs with Extremely Low Roll-Off. *ACS Appl Mater Interfaces* **2021**, *13*, 57713–57724, doi:10.1021/acsami.1c17449.

43. Shizu, K.; Lee, J.; Tanaka, H.; Nomura, H.; Yasuda, T.; Kaji, H.; Adachi, C. Highly Efficient Electroluminescence from Purely Organic Donor–Acceptor Systems. *Pure and Applied Chemistry* **2015**, *87*, 627–638, doi:10.1515/pac-2015-0301.
44. Nishimoto, T.; Yasuda, T.; Lee, S.Y.; Kondo, R.; Adachi, C. A Six-Carbazole-Decorated Cyclophosphazene as a Host with High Triplet Energy to Realize Efficient Delayed-Fluorescence OLEDs. *Mater. Horiz.* **2014**, *1*, 264–269, doi:10.1039/C3MH00079F.
45. Huang, B.; Ban, X.; Sun, K.; Ma, Z.; Mei, Y.; Jiang, W.; Lin, B.; Sun, Y. Thermally Activated Delayed Fluorescence Materials Based on Benzophenone Derivative as Emitter for Efficient Solution-Processed Non-Doped Green OLED. *Dyes and Pigments* **2016**, *133*, 380–386, doi:10.1016/j.dyepig.2016.06.025.
46. Liang, J.; Li, C.; Zhuang, X.; Ye, K.; Liu, Y.; Wang, Y. Novel Blue Bipolar Thermally Activated Delayed Fluorescence Material as Host Emitter for High-Efficiency Hybrid Warm-White OLEDs with Stable High Color-Rendering Index. *Adv Funct Mater* **2018**, *28*, doi:10.1002/adfm.201707002.
47. Pocock, I.A.; Alotaibi, A.M.; Jagdev, K.; Prior, C.; Burgess, G.R.; Male, L.; Grainger, R.S. Direct Formation of 4,5-Disubstituted Carbazoles *via* Regioselective Dilithiation. *Chemical Communications* **2021**, *57*, 7252–7255, doi:10.1039/D1CC02892H.
48. Zhu, X.-D.; Tian, Q.-S.; Zheng, Q.; Tao, X.-C.; Yuan, Y.; Yu, Y.-J.; Li, Y.; Jiang, Z.-Q.; Liao, L.-S. A Sky-Blue Thermally Activated Delayed Fluorescence Emitter Based on Multimodified Carbazole Donor for Efficient Organic Light-Emitting Diodes. *Org Electron* **2019**, *68*, 113–120, doi:10.1016/j.orgel.2019.02.001.
49. Liu, F.; Zou, J.; He, Q.; Tang, C.; Xie, L.; Peng, B.; Wei, W.; Cao, Y.; Huang, W. Carbazole End-capped Pyrene Starburst with Enhanced Electrochemical Stability and Device Performance. *J Polym Sci A Polym Chem* **2010**, *48*, 4943–4949, doi:10.1002/pola.24289.
50. Sęk, D.; Szlapa-Kula, A.; Siwy, M.; Fabiańczyk, A.; Janeczek, H.; Szalkowski, M.; Maćkowski, S.; Schab-Balcerzak, E. Branched Azomethines Based on Tris(2-Aminoethyl)Amine: Impact of Imine Core Functionalization on Thermal, Electrochemical and Luminescence Properties. *Mater Chem Phys* **2020**, *240*, 122246, doi:10.1016/j.matchemphys.2019.122246.
51. Sebris, A.; Novosjolova, I.; Traskovskis, K.; Kokars, V.; Tetervenoka, N.; Vembris, A.; Turks, M. Photophysical and Electrical Properties of Highly Luminescent 2/6-Triazolyl-Substituted Push–Pull Purines. *ACS Omega* **2022**, *7*, 5242–5253, doi:10.1021/acsomega.1c06359.
52. Huang, T.; Jiang, W.; Duan, L. Recent Progress in Solution Processable TADF Materials for Organic Light-Emitting Diodes. *J Mater Chem C Mater* **2018**, *6*, 5577–5596, doi:10.1039/C8TC01139G.
53. Wang, J.; Liu, C.; Jiang, C.; Yao, C.; Gu, M.; Wang, W. Solution-Processed Aggregation-Induced Delayed Fluorescence (AIDF) Emitters Based on Strong π-Accepting Triazine Cores for Highly Efficient Nondoped OLEDs with Low Efficiency Roll-Off. *Org Electron* **2019**, *65*, 170–178, doi:10.1016/j.orgel.2018.11.018.
54. Li, Y.; Xie, G.; Gong, S.; Wu, K.; Yang, C. Dendronized Delayed Fluorescence Emitters for Non-Doped, Solution-Processed Organic Light-Emitting Diodes with High Efficiency and Low Efficiency Roll-off Simultaneously: Two Parallel Emissive Channels. *Chem Sci* **2016**, *7*, 5441–5447, doi:10.1039/C6SC00943C.
55. Sun, S.; Wang, J.; Chen, L.; Chen, R.; Jin, J.; Chen, C.; Chen, S.; Xie, G.; Zheng, C.; Huang, W. Thermally Activated Delayed Fluorescence Enantiomers for Solution-Processed Circularly Polarized Electroluminescence. *J Mater Chem C Mater* **2019**, *7*, 14511–14516, doi:10.1039/C9TC04941J.
56. Inoue, S.; Minemawari, H.; Tsutsumi, J.; Chikamatsu, M.; Yamada, T.; Horiuchi, S.; Tanaka, M.; Kumai, R.; Yoneya, M.; Hasegawa, T. Effects of Substituted Alkyl Chain Length on Solution-Processable Layered Organic Semiconductor Crystals. *Chemistry of Materials* **2015**, *27*, 3809–3812, doi:10.1021/acs.chemmater.5b00810.
57. Vaitkeviciene, V.; Grigalevicius, S.; Grazulevicius, J.V.; Jankauskas, V.; Syromyatnikov, V.G. Hole-Transporting [3,3′]Bicarbazolyl-Based Polymers and Well-Defined Model Compounds. *Eur Polym J* **2006**, *42*, 2254–2260, doi:10.1016/j.eurpolymj.2006.06.023.
58. Gautam, P.; Shahnawaz; Siddiqui, I.; Blazevicius, D.; Krucaite, G.; Tavgeniene, D.; Jou, J.-H.; Grigalevicius, S. Bifunctional Bicarbazole-Benzophenone-Based Twisted Donor–Acceptor–Donor Derivatives for Deep-Blue and Green OLEDs. *Nanomaterials* **2023**, *13*, 1408, doi:10.3390/nano13081408.
59. Blazevicius, D.; Siddiqui, I.; Gautam, P.; Krucaite, G.; Tavgeniene, D.; Nagar, M.R.; Kumar, K.; Banik, S.; Jou, J.-H.; Grigalevicius, S. Bicarbazole-Benzophenone-Based Twisted Donor-Acceptor-Donor Derivatives as Blue Emitters for Highly Efficient Fluorescent Organic Light-Emitting Diodes. *Nanomaterials* **2024**, *14*, 146, doi:10.3390/nano14020146.

60. De Sa Pereira, D.; Data, P.; Monkman, A.P. Methods of Analysis of Organic Light Emitting Diodes. *Display* **2017**, *2*, 323–337.
61. Zhao, L.; Liu, Y.; Wang, S.; Tao, Y.; Wang, F.; Zhang, X.; Huang, W. Novel Hyperbranched Polymers as Host Materials for Green Thermally Activated Delayed Fluorescence OLEDs. *Chinese Journal of Polymer Science* **2017**, *35*, 490–502, doi:10.1007/s10118-017-1881-1.
62. Sworakowski, J. How Accurate Are Energies of HOMO and LUMO Levels in Small-Molecule Organic Semiconductors Determined from Cyclic Voltammetry or Optical Spectroscopy? *Synth Met* **2018**, *235*, 125–130, doi:10.1016/j.synthmet.2017.11.013.